Energy- and crystal momentum-resolved study of laser-induced femtosecond magnetism

G. P. Zhang*
Department of Physics, Indiana State University, Terre Haute, Indiana 47809, USA

Yihua Bai
Center for Instruction, Research and Technology, Indiana State University, Terre Haute, Indiana 47809, USA

Thomas F. George
Office of the Chancellor and Center for Nanoscience, Department of Chemistry & Biochemistry and Department of Physics & Astronomy, University of Missouri–St. Louis, St. Louis, Missouri 63121, USA
(Received 1 July 2009; revised manuscript received 15 October 2009; published 16 December 2009)

When a femtosecond (fs) laser pulse strikes a ferromagnet, it demagnetizes the sample within a few hundred fs but its underlying mechanism has remained elusive for over a decade. Here a possible microscopic picture is revealed through an energy- and crystal momentum-resolved first-principles investigation, first by locating the optimal excitation-energy window for the maximal magnetization change and then mapping out every magnetic contribution from each crystal momentum **k** point along the high-symmetry lines within the Brillouin zone. We find that not all the **k** points contribute evenly, where a few momentum **k** points show a much stronger magnetic-moment change than others. In ferromagnetic nickel, less than 50% of the **k** points contribute over 90% of the magnetization change. By closely examining the transition-matrix elements and spin-moment change associated with those **k** points, we further find the reduction in the dynamical magnetic moment is directly connected with these transition-moments and spin-moment changes between band states.

DOI: 10.1103/PhysRevB.80.214415 PACS number(s): 75.40.Gb, 75.70.−i, 78.20.Ls, 78.47.J−

I. INTRODUCTION

In 1996, Beaurepaire *et al.*[1] demonstrated that a femtosecond (fs) laser pulse can demagnetize a ferromagnetic film within a picosecond. This process is at least three orders of magnitude faster than the existing speed of a magnetic recording and has attracted considerable attention both experimentally[2–4] and theoretically.[5–7] Stanciu *et al.*[8] demonstrated the inverse Faraday effect recently, where the magnetic spin orientation can be switched nonthermally and works even better at cooler temperatures.[9] The spin manipulation is also demonstrated in nanostructures.

Despite extensive investigative efforts, the microscopic origin of femtosecond magnetism or femtomagnetism is still unclear. Our first attempt[5] demonstrated that the spin-orbit coupling (SOC) can cause the demagnetization: SOC opens a spin symmetry-breaking channel while the laser field provides the intensity to induce a substantial magnetic change. Since then, two other theoretical reports[6,7] have been published but their focus is on the time-resolved magneto-optical signal.[10] Recently, the Elliot-Yafet or spin-phonon mechanism[11] was proposed but its role on the shortest time scale is far from obvious. Bigot *et al.*[12] has discussed this issue recently as well. However, it is clear that the intrinsic interplay among the charge, spin, and orbital[13–15] plays a crucial role. Spin-, time-, and energy-resolved two-photon photoemission studies[16,17] showed that the spin-orbit hybridization hot spots enhance spin-flip scattering by several orders of magnitude. This finding is very interesting as it connects the macroscopic magnetization to the microscopic electronic states, and more importantly, it suggests a possibility to resolve magnetic-moment change in the momentum space experimentally.

Motivated by these experimental and theoretical results, in this paper, we shed light on the microscopic origin of femtomagnetism by a joint energy- and crystal momentum-resolved first-principles calculation. We first scan the laser energy to locate the maximum magnetization change. Then, within this optimal laser-energy window, we systematically map out individual magnetic-moment changes from every single-crystal momentum **k** along the high-symmetry lines. A few **k** points, which contribute substantial magnetic-moment changes, emerge. In fcc nickel, they are located along the Γ-X and L-W directions. By looking into the magnetic and electronic structures of these points, we discover that there is a connection between the dynamical magnetic-moment reduction and the static moment change between band states.

This paper is arranged as follows. In Sec. II, we present the theoretical formalism. Then we give the energy requirements in Sec. III. Section IV is devoted to the magnetic requirement, followed by the optical requirement in Sec. V. We present our current understanding and discussion in Sec. VI. A conclusion is presented in Sec. VII. Appendix A shows the details of our implementation of the spin matrix within the full-potential linearized augmented plane-wave basis. Appendix B presents an example of how the spin and transition moments are correlated.

II. THEORETICAL FORMALISM

Our formalism is based on the density-functional theory (DFT). We start with the Kohn-Sham equation (in Ry atomic units)

$$[-\nabla^2 + V_{Ne} + V_{ee} + V_{xc}^{\sigma}]\psi_{i\mathbf{k}}^{\sigma}(r) = E_{i\mathbf{k}}^{\sigma}\psi_{i\mathbf{k}}^{\sigma}(r). \quad (1)$$

The terms on the left-hand side represent the kinetic energy, electron-nuclear attraction, Coulomb, and exchange interac-

tions, respectively. $\psi_{i\mathbf{k}}^{\sigma}(r)$ is the Bloch wave function of band i at crystal momentum $\mathbf{k}$ with spin σ and $E_{i\mathbf{k}}^{\sigma}$ is the band energy. The spin-orbit coupling is included using a second-variational method in the same self-consistent iteration.[18] The spin-mixed wave functions and eigenvalues are denoted as $\tilde{\psi}_{i\mathbf{k}}$ and $\tilde{E}_{i\mathbf{k}}$. We use the full-potential linearized augmented plane-wave (FLAPW) method as implemented in the WIEN2K code.[19]

We take ferromagnetic nickel as our example. The product of the smallest atomic sphere radius in the unit cell and the largest plane-wave vector, or $R_{mt}K_{\max}$, is 9.5.[19] We use the generalized gradient approximation to the exchange-correlation functional. We also compare it with the local-density approximation and we find the net magnetic-moment changes are almost identical for nickel. Our band structure, magnetic, and optical properties are fully consistent with the previous investigations.[6,7] One big challenge in all the optical calculations is the $\mathbf{k}$-point convergence. Although a $\mathbf{k}$ mesh of $87\times87\times87$ is sufficient,[20] to be more convincing, here we use an extremely fine mesh of $104\times104\times104$.

With the presence of a laser field, the system Hamiltonian consists of two parts: one for the system and the other for the interaction between the laser field and the system. For the system, we have

$$H_0 = \sum_{ik} \tilde{E}_{i\mathbf{k}}\rho_{i,i;\mathbf{k}}, \tag{2}$$

where $\rho_{i,i;\mathbf{k}}$ is the density matrix at point $\mathbf{k}$ and $\tilde{E}_{i\mathbf{k}}$ is the eigenvalue of the band state $i\mathbf{k}$. At time $t=0$, $\rho_{i,i;\mathbf{k}}$ is just the occupation number of the band in the ground state. The interaction Hamiltonian can be written as

$$H_I = -e\vec{F}(t)\cdot\sum_{\mathbf{k}}\sum_{ij(i\neq j)}\vec{r}_{ij;\mathbf{k}}\rho_{i,j;\mathbf{k}}, \tag{3}$$

where e is the electron charge. We do not include the magnetic contribution since it is much smaller. $\rho_{i,j;\mathbf{k}}$ is the density-matrix element between states i and j at point $\mathbf{k}$ and is zero at time $t=0$. $\vec{r}_{i,j,;\mathbf{k}}$ is the dipole transition-moment operator between states i and j at crystal momentum $\mathbf{k}$. Since in solids the dipole operator is ill defined,[21] we compute it from the momentum operator $\vec{p}$ using[22–24]

$$\vec{r}_{i,j;\mathbf{k}} = \frac{\hbar\vec{p}_{ij;\mathbf{k}}}{im(\tilde{E}_{i\mathbf{k}}-\tilde{E}_{j\mathbf{k}})}, \tag{4}$$

where m is the electron mass and $\hbar$ is Planck's constant over 2π. Note that optical transitions are associated only with $(\tilde{E}_{i\mathbf{k}}-\tilde{E}_{j\mathbf{k}})\neq0$ and $\vec{p}_{ij;\mathbf{k}}$ is computed by first forming a matrix within the FLAPW basis and then multiplying it with the wave-function coefficients.[22,23,25] These coefficients [see a and b in Eq. (A5)] of the wave functions are computed in the LAPWSO subroutines in the WIEN2K code. $\vec{F}(t)$ is the laser electric field with the laser-pulse shape $|\vec{F}(t)| = A\exp(-t^2/\tau^2)\cos(\omega t)$, where A, ω, t, and τ are the electric field amplitude, laser frequency, time, and laser-pulse duration, respectively.

The time-dependent density matrix $\rho_{i,j;\mathbf{k}}$ is computed from the Liouville equation[10,26]

$$i\hbar\frac{\partial\rho_{i,j;\mathbf{k}}}{\partial t} = (\tilde{E}_{i\mathbf{k}}-\tilde{E}_{j\mathbf{k}})\rho_{i,j;\mathbf{k}} - e\vec{F}(t)\cdot\sum_{m}(\vec{r}_{i,m;\mathbf{k}}\rho_{m,l;\mathbf{k}}-\rho_{i,m;\mathbf{k}}\vec{r}_{m,j;\mathbf{k}}). \tag{5}$$

Within the dipole approximation, equations of different $\mathbf{k}$ do not mix, which is the reason why we can run our code in parallel efficiently. Once we find the density matrix, the magnetic spin moment is computed from

$$M_z(t) = \sum_{\mathbf{k}} Tr(\rho_{\mathbf{k}}S_{\mathbf{k}}^z), \tag{6}$$

where $S_{\mathbf{k}}^z$ is the spin matrix. The details of the spin matrix implementation within the FLAPW basis are presented in Appendix A.

III. ENERGY REQUIREMENT

The very first impact of a laser pulse on a system is that it will preferentially choose an energy window. At first, it creates an initial charge excitation. The center of this excitation is determined by the laser energy, band structure, and optical-transition moment. But whether they will lead to magnetization change or spin excitation is determined by the spin matrix and the spin-orbit coupling. This indirect connection between these two excitations complicates a simple explanation of magnetization change. Even more difficult is that the optical and magnetic excitations have very distinctive properties. The optical transition (within the dipole approximation) is only allowed with $\Delta m_s=0$ if SOC is ignored but the magnetic excitation requires a transition with $(\Delta m_s\neq0)$. Here, Δm_s refers to the magnetic quantum-number change. Therefore, a proper understanding of the delicate balance between these two competing requirements is at the core of femtomagnetism.

We employ a 12-fs laser pulse with a laser field amplitude of 0.05 V/Å.[27] Figure 1 shows the comprehensive picture of magnetic-moment change as a function of time and laser energy. This landscape is constructed with 18 different laser energies with the smallest energy step being 0.025 eV. Different colors are used to highlight the magnetic-moment change. This figure reveals the crucial information about the laser-induced magnetization change. The magnetic-moment change depends on the laser energy with the maximal reduction around $\hbar\omega=2$ eV, where the magnetic moment drops and recovers quickly with a strong oscillation. The period of this oscillation is inversely proportional to the average strength of the spin-orbit coupling associated with the dipole-allowed transitions (see below).[20] This energy requirement results from the band structure, where only a finite-energy region is excitable.[13,20]

The above energy scan narrows down the search window substantially. Next, if we compare this optimal laser energy of 2 eV against the band dispersion [see Fig. 2(a)], we see that energetically quite a few possible transitions potentially match 2 eV across the Brillouin zone but this energy match is not enough for either an optical transition or magnetic-moment change. Figure 2(b) presents our crystal momentum

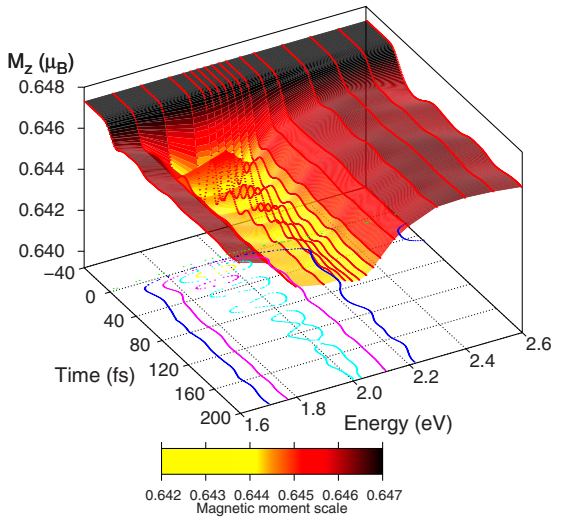

FIG. 1. (Color online) Magnetization change as a function of time and laser energy. 18 laser energies are used: 1.500, 1.600, 1.700, 1.800, 1.900, 1.950, 1.975, 2.000, 2.025, 2.050, 2.075, 2.100, 2.150, 2.200, 2.300, 2.400, 2.500, and 2.600 eV. The laser-pulse duration is 12 fs. The field amplitude is 0.05 V/Å. The dark color represents a larger magnetic moment (see the magnetic-moment scale at the bottom). The optimal laser energy is around 2 eV, where the moment shows a strong oscillation.

k-resolved magnetic-moment change $\Delta M_z^{\mathbf{k}}(t)$ or a magnetic-moment dispersion. This is our major finding. The magnetic-moment change is computed from $\Delta M_z^{\mathbf{k}}(t) = M_z^{\mathbf{k}}(t) - M_z^{\mathbf{k}}(-\infty)$ for each **k** point. Since normally the magnetic moment at each **k** point oscillates with time, we choose their respective troughs (red boxes) and peaks (black circles) for time over 40 fs. For convenience, the moment change is not weighted by the **k**-point weight so that a direct comparison among those changes is possible.

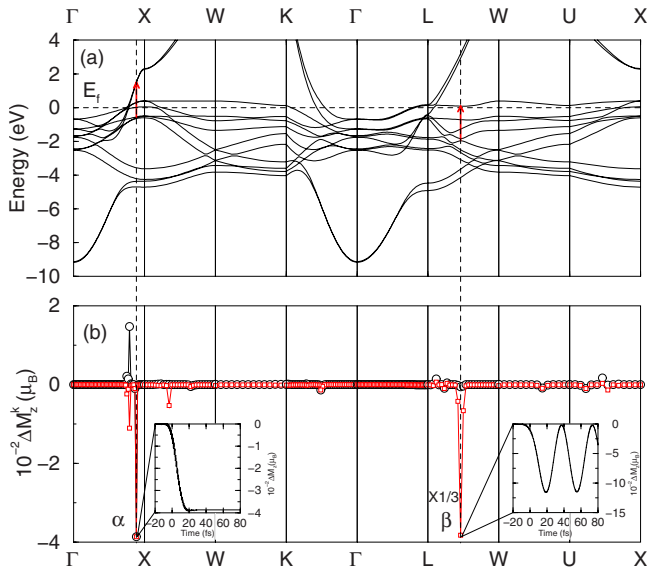

FIG. 2. (Color online) (a) Nickel band structure. The horizontal dashed line denotes the Fermi level. Two vertical dashed lines highlight two **k** points. The relevant transitions are represented by two arrows. (b) Dispersion of the spin-moment change along the high-symmetry lines in the first Brillouin zone. The troughs are indicated by red boxes and the peaks by black circles. The original magnetic moments are subtracted. Two points, denoted by α and β, are along the Γ-X and L-W lines. Their respective time-dependent changes are in the insets. Note that the x axis is plotted disproportionally for clarity.

Our findings are truly distinct. First, not all the symmetry lines contribute equally to the magnetic spin-moment change. There is a small change along the W-K, Γ-L, and W-U directions due to the stringent energy requirements. The maximum changes are along the Γ-X and L-W directions. Along the Γ-X line, there are two **k** points. The magnetic-moment change at the first point shows a strong oscillation between 0.0148 and $-0.0110\mu_B$. Our interest is in the second point, denoted as α, which shows a huge magnetic-moment decrease with little oscillation [see the lower-left inset of Fig. 2(b)]. Its crystal momentum is $(0.8846,0,0)2\pi/a$, where a is the lattice constant of nickel. Along the L-W line, another point, denoted as β, is located at $(0.7308,0.5,0.2692)2\pi/a$. This point shows a huge oscillation [see the lower-right inset around β in Fig. 2(b)] with the trough at $-0.1146\mu_B$ and peak at $-0.00168\mu_B$. We highlight these two points with two vertical dashed lines through Fig. 2 and with two arrows denoting the relevant transitions on the band dispersion in Fig. 2(a). These two points, though neither at a high-symmetry point nor at any special point, hold a long-awaited answer to the ultrafast magnetization change at the earliest time scale.

IV. MAGNETIC REQUIREMENT

Pickel *et al.*[16] already reported the importance of the spin-orbit hybridization points in fcc Co but what differentiates our present study from all the other investigations is that we examine energy, optical, and magnetic properties simultaneously. This is proved to be very critical. Table I shows the energies and spin moments of the eigenstates at points α and β. The Fermi energy is at 0 eV. States with energy far below or above the Fermi energy are not included. We underline the spin moments and energies of those relevant occupied and unoccupied states; all other states are magnetically silent for the current-laser parameters.

We start with point α. One notices immediately that energetically the relevant transitions are from states 5, 6, and 7 to states 11 and 12 since the transition energy is close to our laser energy of 2 eV. Since states 5, 6, 7, and 11 have a similar spin moment of about $0.99\mu_B$, the transitions from states 5, 6, and 7 to 11 lead to a very small moment change. The most important transitions for the magnetization change are from states 5, 6, and 7 to 12. Since state 12 has an opposite spin polarization to those of the other three, any transition leads to a spin flip. Had our process been thermally or magnetically driven, our discussion would end here. Optically, there is a big twist in the argument, which lies at the center of femtomagnetism.

V. OPTICAL REQUIREMENT

In optics, one must obey the dipole-selection rule. If a system has no spin-orbit coupling, the magnetic spin

TABLE I. Eigenenergies and spin moments at **k** points α along the Γ-X line and β along the L-W line. For α, transitions from states 5, 6, and 7 (underlined) to states 11 and 12 (underlined) are the main contributions to the spin-moment change; for β, transitions from states 6 and 7 (underlined) to state 10 (underlined) are the main contribution to the spin-moment change. The Fermi energy is set to zero.

k point α			**k** point β		
Eigenstate	Energy (eV)	Spin (μ_B)	Eigenstate	Energy (eV)	Spin (μ_B)
1	−4.700063	0.999629	1	−4.144899	0.998828
2	−4.366774	−0.999385	2	−3.641940	−0.995499
3	−4.202106	0.998913	3	−3.073408	0.994145
4	−3.562884	−0.997792	4	−2.659985	−0.946254
5	0.649266	0.997968	5	−2.493826	0.950511
6	−0.604067	0.980963	6	−1.955209	0.132567
7	−0.552437	0.984501	7	−1.840904	−0.137636
8	0.020963	−0.990619	8	−1.275453	−0.991536
9	0.299355	−0.982946	9	−0.715007	0.993213
10	0.306642	−0.990310	10	0.088765	−0.998160
11	1.475095	0.998578	11	2.922291	0.999391
12	1.493074	−0.999490	12	3.202704	−0.999515

quantum-number change Δm_s is zero. How does the spin-orbit coupling do the trick to influence the magnetization? Density-functional theory[19] offers a fresh insight. The momentum transition-matrix elements $|D|$ (in atomic units)[23] between those states are as follows: $|D_{5,11}|=0$, $|D_{5,12}|=0.001$, $|D_{6,11}|=0.338$, $|D_{6,12}|=0$, $|D_{7,11}|=0$, and $|D_{7,12}|=0.029$. State 5 is magnetically silent due to its nearly zero dipole-transition element. Two major transitions, one from state 6 to 11 and the other from state 7 to 12, reveal the hidden correlation between the optical transition moment and magnetic-moment change. The transition from state 6 to 11, which has the largest transition moment, has a very small magnetic enhancement of $0.017615\mu_B$. The transition from 7 to 12, which has a small transition moment, has the largest spin moment change of nearly $-2\mu_B$.

VI. CURRENT UNDERSTANDING AND DISCUSSION

The correlation has a simple explanation using the eigenfunctions of the total angular momentum J for a system with spherical symmetry. The eigenfunctions of two different types[14] allow 15 possible transitions, 14 out of which have different dependences of spin momentum change and transition-matrix element (see Appendix B for details). For instance, for the transition $\Delta j=1$, $\Delta m_j=1$, the dipole transition moment (dimensionless) is

$$D=\frac{1}{2}\sqrt{\left(1+\frac{m_j}{j+1}\right)\left(1+\frac{m_j+1}{j+1}\right)} \tag{7}$$

while the spin momentum change ΔS (in units of $\hbar/2$) is

$$\Delta S=\frac{1}{j+1}\left(1-\frac{m_j}{j}\right), \tag{8}$$

where j and m_j are the total and magnetic total angular-momentum numbers, respectively. One can see clearly that D and ΔS have the opposite dependence on m_j, and if D increases, ΔS decreases. The only exception is the transition between two different types of eigenfunctions (see Appendix B). This transition will be very valuable for future magnetization control.

With the above results, we can now explain how the magnetic-moment changes. For point α, the decrease in magnetic moment mainly results from the transition from state 7 to 12, which can be independently verified by switching on and off this transition. The small $7\rightarrow 12$ transition moment reflects that this transition is penalized by the large spin moment change. As a result, the net reduction in magnetic-moment change is only about $-0.039\mu_B$. This is the origin of the demagnetization for α. We can also understand the demagnetization process of point β. Different from α, β shows a strong oscillation. This oscillation comes from the interference between two transitions: one is from state 6 to 10 and the other is from state 7 to 10. Each transition has a transition energy of about 2 eV so they satisfy the energy requirements. The energy difference between states 6 and 7 is 0.114305 eV, which is determined by the spin-orbit coupling. This energy corresponds to a time scale of 36.2 fs, which is exactly the period that we see in the magnetic-moment oscillation of β [see the lower-right inset in Fig. 2(b)].

For the total magnetic-moment change since both pure reductions and oscillatory changes in the magnetic moment are present, a summation over those **k** points leads to the oscillatory reduction in the magnetic moment as seen in Fig. 1. To see how the number of **k** points play a role here in the total magnetic-moment change, we compute the magnetic-moment change as a function of the number of **k** points. We caution that one should not consider this as a mere **k**-point convergence calculation since we use a threshold to pick those points. A usual **k**-point convergence run must use an evenly distributed **k** mesh. We zoom into a small time win-

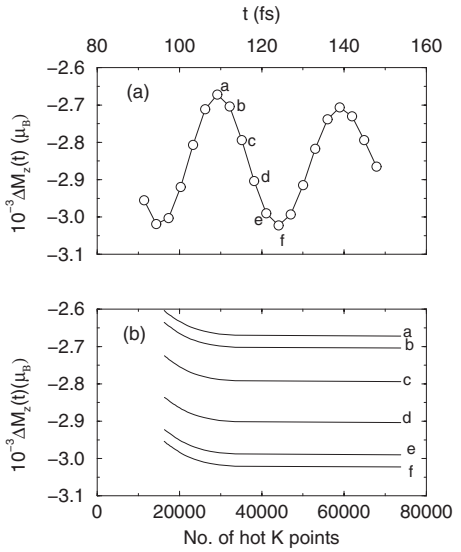

FIG. 3. (a) Spin-magnetic-moment change as a function of time from 90 to 150 fs. The letters from *a* to *f* denote the times examined closely in (b). (b) Contributions of the number of dominant *k* points to the magnetic-moment change. The convergence starts when the number of dominant *k* points reaches 30 000. After that, the change is small. The laser parameters are the same as in Fig. 2.

dow between 90 and 150 fs. Figure 3(a) shows the time evolution of the spin moment change. Here the laser parameters are the same as above. We pick six different times from *a* to *f*. Figure 3(b) shows that when the number of points increases, the moment change starts to converge. We only need 30 000 out of 73 763 points in the irreducible Brillouin zone, or less than 50% points, to achieve over 90% of the magnetic-moment change. The number of points needed is insensitive to the times. From *a* to *f*, we see they almost converge at the same number of hot **k** points. This demonstrates that those points indeed determine the main trend of the magnetic-moment change.

VII. CONCLUSION

In conclusion, our energy- and crystal momentum-resolved study reveals a possible electronic origin of femtomagnetism. By scanning energy and momentum, we find that a few points make a substantial contribution to the magnetic-moment change. By examining the detailed electronic, magnetic, and optical structures of two dominant **k** points, we uncover that a magnetic reduction is already present in their respective transitions. Future experiments can test our predictions by focusing on the Γ-X and L-W lines.

ACKNOWLEDGMENTS

We would like to thank Wolfgang Hübner and Georg Lefkidis (Kaiserslautern, Germany) for numerous discussions and communications. This work was supported by the U.S. Department of Energy under Contract No. DE-FG02-06ER46304 and by a Promising Scholars grant from Indiana State University. In addition, we acknowledge part of the work as done on Indiana State University's high-performance computers. This research used resources of the National Energy Research Scientific Computing Center, which is supported by the Office of Science of the U.S. Department of Energy under Contract No. DE-AC02-05CH11231. Two important calculations used resources of the Argonne Leadership Computing Facility at Argonne National Laboratory, which is supported by the Office of Science of the U.S. Department of Energy under Contract No. DE-AC02-06CH11357.

APPENDIX A: IMPLEMENTATION OF THE SPIN MATRIX IN THE FLAPW BASIS

The calculation of spin dynamics requires the formation of the spin matrix. While it is relatively easy to form in a plane-wave basis, it is a bit complicated within the FLAPW bases with a spin-polarized basis. It is possible to use the same basis functions for both spin-up and spin-down functions, which may ease the difficulty to set up the spin matrix[19,28] but this may compromise the accuracy of the well-converged basis. This is because the FLAPW basis, which is optimized for one spin channel, may not be the optimal basis for another spin channel. So, we decide to use separate basis functions as already implemented in the WIEN2K code. For the reader who is unfamiliar with this code, we refer to the book by Singh and Nordstrom,[29] which we have followed closely when implementing the spin matrix.[28]

The FLAPW method separates a unit cell into spheres and interstitial regions, each of which has different basis functions. The continuity in the value and slope of the basis functions at the sphere boundary connects these two basis functions. Since the basis functions are recalculated in each iteration, the method is very flexible and is among the most accurate methods for a first-principles calculation. For each spin orientation, we get a different basis function. In the following, we label the spin-up function by α and the spin-down one by β (not to be confused with the points α and β in the main text).

To start with, we write down the basis functions for the sphere and the interstitial region as[19]

$$\phi^{\sigma}(\mathbf{k}+\mathbf{K}_n) = \sum_{lm} [A^{\sigma}_{lm}(\mathbf{k}+\mathbf{K}_n)u^{\sigma}_l(r,E_l) + B^{\sigma}_{lm}(\mathbf{k}+\mathbf{K}_n)\dot{u}^{\sigma}_l(r,E_l)]Y_{lm}(\hat{r}) \quad \text{(sphere)}, \quad \text{(A1)}$$

$$\phi^{\sigma}(\mathbf{k}+\mathbf{K}_n) = \frac{1}{\sqrt{\Omega}}\exp[i(\mathbf{k}+\mathbf{K}_n)\cdot\mathbf{r}], \quad \text{(interstitial)}, \quad \text{(A2)}$$

where the **r** dependence in ϕ^{σ} is omitted, σ represents the spin α or β, and A_{lm} and B_{lm} are obtained by requiring that this basis function matches the value and slope of the plane wave at the surface of the sphere or $r=R_{mt}$. This is the only step by which the basis function within the sphere acquires the **k** dependence. u_l is the radial solution of the radial Schrödinger equation at the linearization energy E_l and $\dot{u}_l$ is its energy derivative.[29] Ω is the unit-cell volume and $Y_{lm}(\hat{r})$

is the spherical harmonic centered at the atom. **k** is the wave vector inside the first Brillouin zone and $\mathbf{K}_n$ is the nth reciprocal-lattice vector. Therefore, the spin-wave functions of state $l\mathbf{k}$ are expanded as

$$\psi^{\sigma}_{l\mathbf{k}} = \sum_{\mathbf{K}_n} c^{l\mathbf{k},\sigma}_{\mathbf{K}_n} \phi^{\sigma}(\mathbf{k}+\mathbf{K}_n). \tag{A3}$$

With presence of the spin-orbit coupling, the states mix spin-up and spin-down characters. We consider the spin matrix between two states, $\tilde{\psi}_{i\mathbf{k}}$ and $\tilde{\psi}_{j\mathbf{k}}$

$$\tilde{\psi}_{i\mathbf{k}} = \sum_{l_1} a^{i\alpha}_{l_1,\mathbf{k}} \psi^{\alpha}_{l_1\mathbf{k}}(r)|\alpha\rangle + \sum_{l_2} b^{i\beta}_{l_2,\mathbf{k}} \psi^{\beta}_{l_2\mathbf{k}}(r)|\beta\rangle, \tag{A4}$$

$$\tilde{\psi}_{j\mathbf{k}} = \sum_{J_1} a^{j\alpha}_{J_1,\mathbf{k}} \psi^{\alpha}_{J_1\mathbf{k}}(r)|\alpha\rangle + \sum_{J_2} b^{j\beta}_{J_2,\mathbf{k}} \psi^{\beta}_{J_2\mathbf{k}}(r)|\beta\rangle, \tag{A5}$$

where a and b are the coefficients of the wave functions computed in the LAPWSO subroutines in the WIEN2K code. They characterize the degree of the spin mixing. The simplest spin matrix is the S_z matrix (unit of the Bohr magneton)

$$\langle\tilde{\psi}_{i\mathbf{k}}|S_z|\tilde{\psi}_{j\mathbf{k}}\rangle = \sum_{I} (a^{i\alpha}_{I\mathbf{k}})^* a^{j\alpha}_{I\mathbf{k}} - \sum_{J} (b^{i\beta}_{J\mathbf{k}})^* b^{j\beta}_{J\mathbf{k}}, \tag{A6}$$

where we have already used the orthogonality property in Eqs. (A4) and (A5). These two summations may have different dimensions since they belong to different spin subspaces. The major implementation difficulty comes from S_x and S_y. We first realize that $S_x=(S^+ + S^-)/2$ and $S_y=(S^+ - S^-)/2i$. Therefore, we only need form the matrix elements $\langle\tilde{\psi}_{i\mathbf{k}}|S^+|\tilde{\psi}_{j\mathbf{k}}\rangle$ and $\langle\tilde{\psi}_{i\mathbf{k}}|S^-|\tilde{\psi}_{j\mathbf{k}}\rangle$. Using Eqs. (A4) and (A5), we find the following two expressions:

$$\langle\tilde{\psi}_{i\mathbf{k}}|S^+|\tilde{\psi}_{j\mathbf{k}}\rangle = \sum_{I,J} (a^{i\alpha}_{I\mathbf{k}})^* b^{j\beta}_{J\mathbf{k}} \langle\psi^{\alpha}_{I\mathbf{k}}(r)|\psi^{\beta}_{J\mathbf{k}}(r)\rangle, \tag{A7}$$

$$\langle\tilde{\psi}_{i\mathbf{k}}|S^-|\tilde{\psi}_{j\mathbf{k}}\rangle = \sum_{I,J} (b^{i\beta}_{J\mathbf{k}})^* a^{j\alpha}_{I\mathbf{k}} \langle\psi^{\beta}_{I\mathbf{k}}(r)|\psi^{\alpha}_{J\mathbf{k}}(r)\rangle, \tag{A8}$$

where the matrix elements $\langle\psi^{\alpha}_{I\mathbf{k}}(r)|\psi^{\beta}_{J\mathbf{k}}(r)\rangle$ and $\langle\psi^{\beta}_{I\mathbf{k}}(r)|\psi^{\alpha}_{J\mathbf{k}}(r)\rangle$ are computed from Eq. (A3).

The only integrations that have to be evaluated are those between the FLAPW basis functions. This in turn boils down to the integrations between the u and $\dot{u}$ functions and plane-wave functions in Eqs. (A1) and (A2), in the same fashion as the overlap matrix. The only difference is that here we have many more terms since integrals such as $\langle u^{\alpha}|u^{\beta}\rangle$ are no longer equal to one and $\langle u^{\alpha}|\dot{u}^{\beta}\rangle$ are no longer zero. The computation of the plane-wave part stays the same. For the local orbitals, we implement this in the same way.

APPENDIX B: SPIN MOMENTUM AND DIPOLE-TRANSITION MOMENT IN A SPHERICAL SYSTEM

We start with the eigenfunctions of the total angular momentum J. They are also the eigenfunctions of the spin-orbit coupling. In solids, they become the basis states for any Bloch states. A detailed investigation of these eigenfunctions is of great importance to understand how the spin-momentum change correlates with the transition-matrix elements. Since all the calculations are analytic, this removes any numerical uncertainty. In principle, the eigenfunction should include the radial part of the wave function but for a fixed orbital quantum number l they only contribute a prefactor and do not affect the trend in transition moments and spin-momentum change. So we ignore them in the following discussion. We will show exactly how for most transitions, the spin-momentum change[14] and transition-matrix element are mutually competing.

For $j=l+1/2$ and $m_j=m+1/2$, the eigenfunction is

TABLE II. Dipole-transition moments D and spin-momentum changes ΔS (in units of $\hbar/2$) for 15 possible transitions. The contribution from the radial wave function is not included.

Transition	$\psi_a \rightarrow \psi'_a$	
$m_{j'}-m_j$ \ $j'-j$	1	−1
1	$D=\frac{1}{2}\sqrt{(1+\frac{m_j}{j+1})(1+\frac{m_j+1}{j+1})}$ $\Delta S=\frac{1}{j+1}(1-\frac{m_j}{j})$	$D=-\frac{1}{2}\sqrt{(1-\frac{m_j}{j})(1-\frac{m_j+1}{j})}$ $\Delta S=\frac{1}{j-1}(1+\frac{m_j}{j})$
0	$D=\frac{1}{2}\sqrt{(1+\frac{m_j}{j+1})(1-\frac{m_j}{j+1})}$ $\Delta S=-\frac{m_j}{j(j+1)}$	$D=\frac{1}{2}\sqrt{(1+\frac{m_j}{j})(1-\frac{m_j}{j})}$ $\Delta S=\frac{m_j}{j(j-1)}$
−1	$D=-\frac{1}{2}\sqrt{(1-\frac{m_j}{j+1})(1-\frac{m_j-1}{j+1})}$ $\Delta S=-\frac{1}{j+1}(1+\frac{m_j}{j})$	$D=\frac{1}{2}\sqrt{(1+\frac{m_j}{j})(1+\frac{m_j-1}{j})}$ $\Delta S=-\frac{1}{j-1}(1-\frac{m_j}{j})$
Transition	$\psi_b \rightarrow \psi'_b$	
$m_{j'}-m_j$ \ $j'-j$	1	−1
1	$D=\frac{1}{2}\sqrt{(1+\frac{m_j}{j+1})(1+\frac{m_j+1}{j+1})}$ $\Delta S=-\frac{1}{j+2}(1-\frac{m_j}{j+1})$	$D=-\frac{1}{2}\sqrt{(1-\frac{m_j}{j})(1-\frac{m_j+1}{j})}$ $\Delta S=-\frac{1}{j}(1+\frac{m_j}{j+1})$
0	$D=\frac{1}{2}\sqrt{(1+\frac{m_j}{j+1})(1-\frac{m_j}{j+1})}$ $\Delta S=\frac{m_j}{(j+1)(j+2)}$	$D=\frac{1}{2}\sqrt{(1+\frac{m_j}{j})(1-\frac{m_j}{j})}$ $\Delta S=-\frac{m_j}{j(j+1)}$
−1	$D=-\frac{1}{2}\sqrt{(1-\frac{m_j}{j+1})(1-\frac{m_j-1}{j+1})}$ $\Delta S=\frac{1}{j+2}(1+\frac{m_j}{j+1})$	$D=\frac{1}{2}\sqrt{(1+\frac{m_j}{j})(1+\frac{m_j-1}{j})}$ $\Delta S=\frac{1}{j}(1-\frac{m_j}{j+1})$
Transition	$\psi_a \rightarrow \psi_b$	
$m_{j'}-m_j$ \ $j'-j$	0	
1	$D=\frac{1}{2(j+1)}\sqrt{(1-\frac{m_j}{j})(1+\frac{m_j+1}{j})}$ $\Delta S=-\frac{1}{j+1}[1+\frac{(2j+1)m_j}{j}]$	
0	$D=-\frac{m_j}{2j(j+1)}$ $\Delta S=-\frac{(2j+1)m_j}{j(j+1)}$	
−1	$D=\frac{1}{2(j+1)}\sqrt{(1+\frac{m_j}{j})(1-\frac{m_j-1}{j})}$ $\Delta S=\frac{1}{j+1}[1-\frac{(2j+1)m_j}{j}]$	

$$\psi_a = \sqrt{\frac{l+m+1}{2l+1}} Y_{lm}|\alpha\rangle + \sqrt{\frac{l-m}{2l+1}} Y_{lm+1}|\beta\rangle, \quad \text{(B1)}$$

where $|\alpha\rangle$ and $|\beta\rangle$ refer to the spin-up and spin-down eigenstates, and Y_{lm} is spherical harmonic with angular and magnetic angular quantum number l and m, respectively. For $j=l-1/2$ and $m_j=m+1/2$, the eigenfunction is

$$\psi_b = -\sqrt{\frac{l-m}{2l+1}} Y_{lm}|\alpha\rangle + \sqrt{\frac{l+m+1}{2l+1}} Y_{lm+1}|\beta\rangle. \quad \text{(B2)}$$

Note that l and m in Eqs. (B1) and (B2) may differ from each other.

There are fifteen possible transitions: $\psi_{a_1} \rightarrow \psi_{a_2}$ ($\Delta j = \pm 1$, $\Delta m_j = 0, \pm 1$), $\psi_{b_1} \rightarrow \psi_{b_2}$ ($\Delta j = \pm 1$, $\Delta m_j = 0, \pm 1$), and $\psi_a \rightarrow \psi_b$ ($\Delta j = 0$, $\Delta m_j = 0, \pm 1$). The transition-matrix elements D and the spin-momentum change ΔS are listed in Table II, where we see a few common features. First of all, the $\psi_a \rightarrow \psi'_a$ and $\psi_b \rightarrow \psi'_b$ transitions have the same transition-matrix elements, independent of Δj and Δm_j. But the transition-matrix elements D and spin-momentum change ΔS have opposite dependence on m_j. This is reflected in their sign difference. For circularly polarized light, the spin-momentum change consists of two terms. If these two terms have opposite signs then the transition-moment-matrix elements have the same signs in their square roots. For linearly polarized light, ΔS has one term while D always has two terms with opposite signs. The intimate relation between ΔS and D holds true for both the $\psi_a \rightarrow \psi'_a$ and $\psi_b \rightarrow \psi'_b$ transitions.

For the $\psi_a \rightarrow \psi_b$ transition, for circularly polarized light, the relation between the spin-momentum change and transition-dipole moment remains alike. However, for linearly polarized light, the transition moment and spin-momentum change have the same dependence on m_j. The reason is that the spin coefficient of the eigenfunction matches the coefficient of the transition-matrix element. Physically, this match comes from the fact that the transition only changes l not m. Although the $\psi_a \rightarrow \psi_a$ and $\psi_b \rightarrow \psi_b$ transitions have the same opportunities, their spin coefficients of the eigenfunctions are squared, which leads to the mismatch.

In a solid, our main conclusion is still valid. For instance, when we plot nearly a half million points of transition moment versus the spin-moment change along Γ-X direction, we find that when the transition moment becomes larger, the spin-momentum change becomes smaller for most of the transitions. Due to the huge file size, we do not provide this with the paper but readers who are interested in the figure may directly contact the authors.

*gpzhang@indstate.edu

[1] E. Beaurepaire, J.-C. Merle, A. Daunois, and J.-Y. Bigot, Phys. Rev. Lett. **76**, 4250 (1996).

[2] L. Guidoni, E. Beaurepaire, and J.-Y. Bigot, Phys. Rev. Lett. **89**, 017401 (2002).

[3] G. P. Zhang, W. Hübner, E. Beaurepaire, and J.-Y. Bigot, Top. Appl. Phys. **83**, 245 (2002).

[4] J.-Y. Bigot, L. Guidoni, E. Beaurepaire, and P. N. Saeta, Phys. Rev. Lett. **93**, 077401 (2004); M. Vomir, L. H. F. Andrade, L. Guidoni, E. Beaurepaire, and J.-Y. Bigot, *ibid.* **94**, 237601 (2005); I. Radu, G. Woltersdorf, M. Kiessling, A. Melnikov, U. Bovensiepen, J.-U. Thiele, and C. H. Back, *ibid.* **102**, 117201 (2009); B. Koopmans, M. van Kampen, J. T. Kohlhepp, and W. J. M. de Jonge, *ibid.* **85**, 844 (2000); C. Stamm, T. Kachel, N. Pontius, R. Mitzner, T. Quast, K. Holldack, S. Khan, C. Lupulescu, E. F. Aziz, M. Wietstruk, H. A. Dürr, and W. Eberhardt, Nature Mater. **6**, 740 (2007); G. M. Müller, J. Walowski, M. Djordjevic, G. X. Miao, A. Gupta, A. V. Ramos, K. Gehrke, V. Moshnyaga, K. Samwer, J. Schmalhorst, A. Thomas, A. Hütten, G. Reiss, J. S. Moodera, and M. Münzenberg, *ibid.* **8**, 56 (2009).

[5] G. P. Zhang and W. Hübner, Phys. Rev. Lett. **85**, 3025 (2000); W. Hübner and G. P. Zhang, Phys. Rev. B **58**, R5920 (1998); G. P. Zhang and W. Hübner, J. Appl. Phys. **85**, 5657 (1999).

[6] P. M. Oppeneer and A. Liebsch, J. Phys.: Condens. Matter **16**, 5519 (2004).

[7] A. Vernes and P. Weinberger, Phys. Rev. B **71**, 165108 (2005).

[8] C. D. Stanciu, F. Hansteen, A. V. Kimel, A. Kirilyuk, A. Tsukamoto, A. Itoh, and Th. Rasing, Phys. Rev. Lett. **99**, 047601 (2007).

[9] J. Hohlfeld, C. D. Stanciu, and A. Rebei, Appl. Phys. Lett. **94**, 152504 (2009).

[10] G. P. Zhang, W. Hübner, G. Lefkidis, Y. Bai, and T. F. George, Nat. Phys. **5**, 499 (2009).

[11] D. Steiauf and M. Fähnle, Phys. Rev. B **79**, 140401(R) (2009); R. J. Elliott, Phys. Rev. **96**, 266 (1954); Y. Yafet, Solid State Phys. **14**, 1 (1963) A paper by Koopmans *et al.* suggests that the total amount of angular-momentum transfer is limited by the number of photons involved in the laser field. For details, see B. Koopmans, M. van Kampen, and W. J. M. deJonge, J. Phys.: Condens. Matter **15**, S723 (2003).

[12] J.-Y. Bigot, M. Vomir, and E. Beaurepaire, Nat. Phys. **5**, 515 (2009).

[13] G. P. Zhang, Phys. Rev. Lett. **101**, 187203 (2008).

[14] G. P. Zhang and T. F. George, Phys. Rev. B **78**, 052407 (2008).

[15] M. I. Kurkin, N. B. Bakulina, and R. V. Pisarev, Phys. Rev. B **78**, 134430 (2008).

[16] M. Pickel, A. B. Schmidt, F. Giesen, J. Braun, J. Minár, H. Ebert, M. Donath, and M. Weinelt, Phys. Rev. Lett. **101**, 066402 (2008).

[17] T. Kampfrath, R. G. Ulbrich, F. Leuenberger, M. Münzenberg, B. Sass, and W. Felsch, Phys. Rev. B **65**, 104429 (2002).

[18] One should not confuse the variational method with perturbation theory. See the variational method in A. Messiah, *Quantum Mechanics* (Dover, New York, 1999), Chap. No. XVIII, p. 762; see the perturbation method in Chapters XVI and XVII in the same book.

[19] P. Blaha, K. Schwarz, G. K. H. Madsen, D. Kvasnicka, and J. Luitz, *WIEN2K, An Augmented Plane Wave Plus Local Orbitals Program for Calculating Crystal Properties* (Karlheinz Schwarz, Technische Universität Wien, Austria, 2001).

[20] T. Hartenstein, G. Lefkidis, W. Hübner, G. P. Zhang, and Y. Bai, J. Appl. Phys. **105**, 07D305 (2009); G. P. Zhang, Y. Bai, W. Hübner, G. Lefkidis, and T. F. George, *ibid.* **103**, 07B113 (2008).

[21] For other methods to compute the dipole transition matrix in solids, please refer to G. F. Bertsch, J.-I. Iwata, A. Rubio, and K. Yabana, Phys. Rev. B **62**, 7998 (2000); R. Resta and D. Vanderbilt, in *Physics of Ferroelectrics: a Modern Perspective*, edited by K. M. Rabe, C. H. Ahn, and J.-M. Triscone (Springer-Verlag, Berlin, 2007), pp. 31–68; I. Souza, J. Iniguez, and D. Vanderbilt, Phys. Rev. B **69**, 085106 (2004); R. Resta, Phys. Rev. Lett. **80**, 1800 (1998).

[22] S. Sharma, J. K. Dewhurst, and C. Ambrosch-Draxl, Phys. Rev. B **67**, 165332 (2003).

[23] C. Ambrosch-Draxl and J. O. Sofo, Comput. Phys. Commun. **175**, 1 (2006).

[24] We have not included the relativistic corrections in the momentum operator as Wang and Callaway have already pointed out that the matrix element is small [C. S. Wang and J. Callaway, Phys. Rev. B **9**, 4897 (1974)].

[25] Note that the coefficients are spin-orbit coupling dependent. As a result, the transition-matrix element contains the mixed spin-up and spin-down components. One should not confuse the following three matrices: (a) the matrix formed within the LAPW basis, (b) the matrix formed within the spin-polarized basis, and (c) the matrix formed within the spin-polarized basis with the presence of spin-orbit coupling.

[26] There is no intrinsic limitation in our scheme. As far as the DFT works, the scheme will work. If the laser is too strong and melts the sample then our scheme will break down as does the experimental one. We only consider the electron dynamics and work on the time scale of several hundred femtoseconds before the phonon is strongly activated. We can not use temperature concept during the laser excitation: temperature is a statistical concept and should not be used within a few hundred fs.

[27] The small magnetization change is due to a weak laser field used in our simulation. If we use a strong laser, the demagnetization will of course be larger. There are two reasons why we choose a weak laser. First, when excited with a weak laser field, all the states, that make substantial magnetic contribution will make substantial contributions to the magnetic changes when the laser field becomes strong. But the other way around is not necessarily true. We use linearly polarized light in the present work. In metals, polarity does not play a big role since the orbital moment is small. Since our sample is a metal, there is no big effect on the results, which is already known from experiments. The laser affects the system through the second term as explained in our paper (Ref. 14).

[28] C. Ambrosch-Draxl, P. Novak, D. J. Singh, and P. Blaha (private communications).

[29] D. Singh and L. Nordstrom, *Planewaves, Pseudopotentials and the LAPW Method*, 2nd ed. (Springer, Berlin, 2006).